ARL-TR-95-30

Copy No. 14

Backscatter Analysis from a Smooth Sand Surface: Diffusion Approximation

Final Report under Contract N00039-91-C-0082
TD No. 01A2082, Volume Backscatter from Sand Grains

Nicholas P. Chotiros
Adrienne M. Mautner
Julia Laughlin

Applied Research Laboratories
The University of Texas at Austin
P. O. Box 8029 Austin, TX 78713-8029

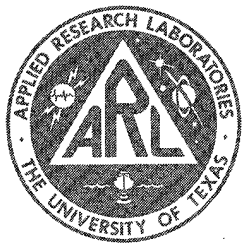

26 October 1995

Final Report

21 June 1994 - 30 June 1995

Approved for public release;
distribution is unlimited

Prepared for:
Naval Research Laboratory
Stennis Space Center, MS 39529-5004

Monitored by:
Space and Naval Warfare Systems Command
Department of the Navy
Arlington, VA 22245-5200

REPORT DOCUMENTATION PAGE

Form Approved
OMB No. 0704-0188

1. AGENCY USE ONLY (Leave blank)	2. REPORT DATE	3. REPORT TYPE AND DATES COVERED
	26 Oct 95	final 21 Jun 94 - 30 Jun 95

4. TITLE AND SUBTITLE

Backscatter Analysis from a Smooth Sand Surface: Diffusion Approximation, Final Report under Contract N00039-91-C-0082, TD No. 01A2082, Volume Backscatter from Sand Grains

5. FUNDING NUMBERS

N00039-91-C-0082,
TD No. 01A2082

6. AUTHOR(S)

Chotiros, Nicholas P. Mautner, Adrienne M. Laughlin, Julia

7. PERFORMING ORGANIZATION NAMES(S) AND ADDRESS(ES)

Applied Research Laboratories
The University of Texas at Austin
P.O. Box 8029
Austin, Texas 78713-8029

8. PERFORMING ORGANIZATION REPORT NUMBER

ARL-TR-95-30

9. SPONSORING/MONITORING AGENCY NAME(S) AND ADDRESS(ES)

Naval Research Laboratory
Stennis Space Center, MS 39529-5004

Space and Naval Warfare Systems Command
Department of the Navy
Arlington, VA 22245-5200

10. SPONSORING/MONITORING AGENCY REPORT NUMBER

11. SUPPLEMENTARY NOTES

12a. DISTRIBUTION/AVAILABILITY STATEMENT

Approved for public release; distribution is unlimited.

12b. DISTRIBUTION CODE

13. ABSTRACT (Maximum 200 words)

The development of a model of backscatter from a smooth underwater sediment surface is described. The model includes two components: the propagation of acoustic energy through the water/sediment interface which is governed by wave theory, and randomization of acoustic energy within the interior of the sediment which is approximated by the diffusion equation. With respect to the wave theory, Biot's poroelastic wave propagation theory is used. The model gives predictions of acoustic backscattering strength as a function of grazing angle, grain size, and energy decay rates that can be matched to experimental data.

14. SUBJECT TERMS

acoustic sand
diffusion scatter
multiple sediment

15. NUMBER OF PAGES

39

16. PRICE CODE

17. SECURITY CLASSIFICATION OF REPORT	18. SECURITY CLASSIFICATION OF THIS PAGE	19. SECURITY CLASSIFICATION OF ABSTRACT	20. LIMITATION OF ABSTRACT
UNCLASSIFIED	UNCLASSIFIED	UNCLASSIFIED	SAR

This page intentionally left blank.

TABLE OF CONTENTS

This page intentionally left blank.

LIST OF FIGURES

This page intentionally left blank.

1. INTRODUCTION

A review of existing bottom backscattering models that are based on sediment volume scattering was made at the beginning of this project. Nolle et al.[1] measured bottom backscattering strength of water saturated sand in a well-controlled laboratory experiment and put forward a bottom backscattering model, in which the sediment is treated as an elastic and lossy liquid. Using the appropriate values for sound speed and attenuation in sand, it is apparent that the model predicts a sharp reduction in backscattering strength below the critical grazing angle. This feature is conspicuously absent from the corresponding laboratory measurements. Both the theory and experimental results are shown in Fig. 1.1. This approach is essentially the same as that of Jackson[2,3] as far as scattering from smooth sediments is concerned. More recently, Hines[4] attempted to introduce an additional mechanism that would alleviate the discrepancy, i.e., the coupling of acoustic energy into the sediment via the evanescent wave, also shown in Fig. 1.1. Doubts concerning the validity of Hines's formulation aside, the model still falls short of agreement with the laboratory data.

It is our hypothesis that there are two flaws in the above models:[1-4] (1) the approximation of the sediment as a liquid, which breaks down at grazing angles below the critical value, and (2) the single scatter approximation, which is invalid where there are numerous scatterers in close proximity to each other, in this case the sand grains themselves. By using the poroelastic wave theory of Biot, and the diffusion equation, it is our intention to formulate a simple, but approximate, theory that can properly explain the experimental data.

The analysis for the acoustic backscatter from a smooth sand surface utilizing the diffusion equation is illustrated in Fig. 1.2. An acoustic pulse of energy originating in the water transmits across the sand/water interface. Once the acoustic pulse is within the sandy sediment, the energy diffuses away from the pulse, some of which reaches the interface and radiates back into the water.

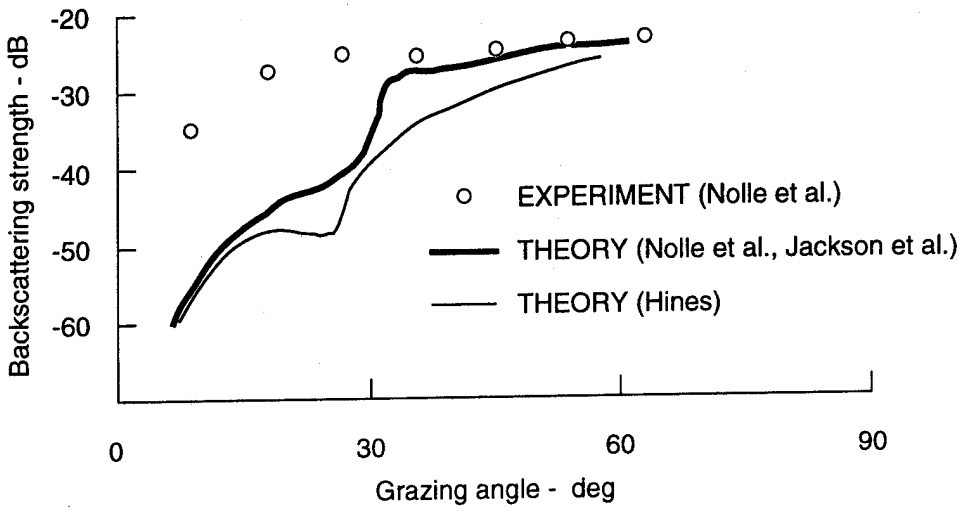

Figure 1.1
Review of existing models.

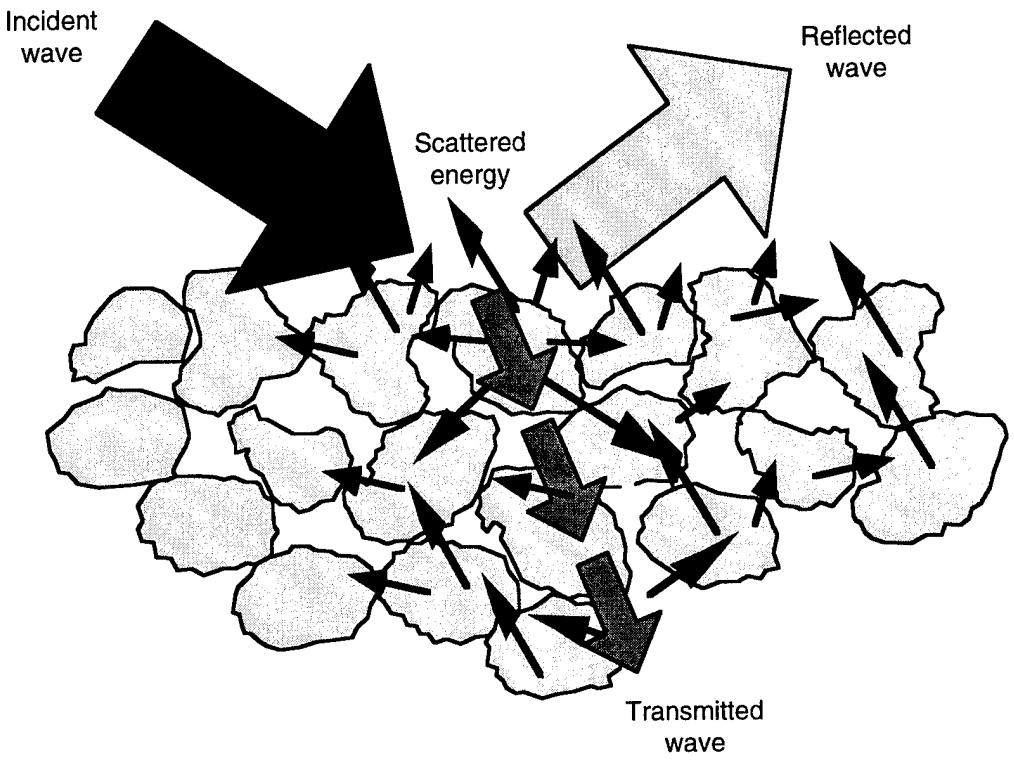

Figure 1.2
Illustration of diffusion model of scattering in sandy sediments.

The assumption which therefore must be made is that the sand grains are in contact with one another to allow the energy to be diffused through them. Once the equation for the diffused energy within the sand has been established, the energy must be computed as it travels through time and space and the necessary constants must be determined.

2. THE DIFFUSION EQUATION

The diffusion equation has been used in modeling ultrasonic scattering in a number of problems, including suspensions,[5] polycrystals,[6] and plates.[7] It is an approximation that is most appropriate for multiple scattering problems where interference between scatterers renders the single scatter approximation untenable. Due to the high density of scatterers and their close proximity, the scattering of sound by sand grains in sandy ocean sediments is also expected to be a multiple scattering problem that should be modeled as a diffusion process. The theoretical derivation is as follows.

Given a density function u of diffuse energy, the net energy flux $\boldsymbol{E}$ is in the opposite direction to the gradient of u,

$$\boldsymbol{E} = -(\nabla u)\alpha^2 \quad , \tag{2.1}$$

where α^2 is the diffusion constant. In the lossless case, the rate of change of u is then given by

$$\frac{\partial}{\partial t}u = \alpha^2\left(\nabla^2 u\right) \quad . \tag{2.2}$$

In the case of lossy diffusion, there will be a decay proportional to u due to absorption, represented by a decay coefficient γ^2. In addition, there may also be an energy source density term F. The lossy diffusion equation with a source density term is given by

$$\frac{\partial}{\partial t}u = \alpha^2(\nabla^2 u) - \gamma^2 u + F \quad . \tag{2.3}$$

Let us consider two cases: the steady state plane wave case and the normally incident plane wave pulse. These two cases are particularly revealing of the physical processes. The first will show the dependence of the scattering strength as a function of grazing angle on physical parameters of the medium. The

second shows the temporal behavior of the diffusion process. Finally, the practical matter of estimating the values of the input parameters is considered.

2.1 STEADY STATE PLANE WAVE CASE

In the steady state case, there is no change as a function of time; therefore Eq. (2.3) reduces to

$$(\nabla^2 u)\alpha^2 - \gamma^2 u + F = 0 \quad . \tag{2.4}$$

For a plane wave propagating in the *x*-*y* plane, in which the *x* axis is horizontal, and the *y* axis vertical, there would be no change in the *x* direction. All variables may be expressed as functions of *y*. Given that solutions in the form of exponential functions are known to exist, let us express *u* in terms of a Fourier transform,

$$u = \int_{-\infty}^{\infty} (Ae^{iky})dk \quad . \tag{2.5}$$

Substituting into the steady state lossy diffusion equation, an expression relating *F* and *A* is obtained,

$$F = \int_{-\infty}^{\infty} ([\alpha^2 k^2 + \gamma^2]Ae^{iky})dk \quad . \tag{2.6}$$

The source density *F* arises from energy that diffuses away from the incident wave, at a rate that is proportional to the intensity of the incident wave. Since the incident wave decreases exponentially with depth, the source density must also decrease exponentially. Let the sand/water interface be at y=0, values of y less than zero being in the sand. Let us further assume that the energy that diffuses to the interface is completely reradiated into the water, which implies that the interface behaves as an energy sink. Then, source density may be modeled as

$$F = \begin{cases} e^{\beta y} & (y < 0) \\ -e^{-\beta y} & (y \geq 0) \end{cases} \quad . \tag{2.7}$$

The source density for values of *y* less than zero is genuine. The source density for *y* values greater than zero is a construction that effectively makes the interface into an energy sink; the antisymmetry ensures that the energy density *u* is always zero at the interface. The source density may also be expressed as a Fourier transform.

$$F = \int_{-\infty}^{\infty} (Be^{iky})dk \quad . \tag{2.8}$$

Substituting from Eq. (2.8) into (2.7), and solving the integral, the Fourier coefficient *B* is given by

$$B = \frac{1}{2\pi}\left(2\frac{ik}{[ik+\beta][-ik+\beta]}\right) \quad . \tag{2.9}$$

Comparing Eqs. (2.6) and (2.8), the following relationship between the Fourier coefficients of the source density and energy density is found.

$$(\alpha^2 k^2 + \gamma^2)A = B \tag{2.10}$$

Eliminating B, an expression for A in terms of the independent variables is found

$$A = \frac{ik}{\pi(ik+\beta)(-ik+\beta)(\alpha^2 k^2 + \gamma^2)} \quad . \tag{2.11}$$

Of particular interest is the rate of diffusion of energy from the sand towards the sand/water interface. The energy flux is related to energy density by Eq. (2.1). Substituting for *A* in Eq. (2.5) from (2.11), then for *u* in Eq. (2.1) from (2.5), solving the Fourier integral, and then setting y=0, the energy flux towards the sand-water interface is found to be

$$E = \frac{\alpha}{\gamma + \alpha\ \beta} \quad . \tag{2.12}$$

The energy flux into the sand from the sand/water interface is given by

$$I = \int_{-\infty}^{0} F \, dy = \frac{1}{\beta} \quad . \tag{2.13}$$

Thus, the energy flux moving towards the interface per unit energy flux moving towards the interior of the sand is given by

$$\frac{E}{I} = \frac{\alpha \beta}{\gamma + \alpha \beta} \quad . \tag{2.14}$$

Scattering strength is defined as scattered power per unit solid angle per unit area per unit incident intensity. In terms of *E* and *I*, the bistatic scattering strength *S* is given by

$$S = \frac{E}{I} \phi(\theta_i)(2\sin[\theta_o]) \frac{\sin(\theta_i)}{2\pi}$$

$$= \frac{\alpha \beta \sin(\theta_i) \phi(\theta_i) \sin(\theta_o)}{(\gamma + \alpha \beta)\pi} \quad , \tag{2.15}$$

where $\phi(\theta_i)$ is the plane wave intensity transmission coefficient from water into sediment at a grazing angle θ_i; $2\sin(\theta_o)$ is the intensity transmission coefficient from sand to water from a baffled aperture that is very much smaller than a wavelength, at an exit angle θ_o relative to the horizontal; $\phi(\theta_i)$ is determined by elastic wave theory for an elastic sediment, or by Biot's theory for porous sediment such as sand. Thus, a very simple expression for the bistatic scattering strength has been obtained in terms of the diffusivity α, decay coefficient of the coherent wave as a function of depth β, and the absorption coefficient of the diffuse energy γ.

2.2. NORMALLY INCIDENT PLANE WAVE PULSE

Consider a Gaussian shaded pulse of width *a* traveling in the negative *y* direction at a speed *c*. With reference to Eq. (2.3), the source function may be expressed as

$$F = e^{-\left(\frac{y + c\,s}{a}\right)^2 - \beta\, c\, s}\, \delta(t - s) \quad , \tag{2.16}$$

where δ is the delta function. This expression was chosen to allow the diffusion to be solved in a stepwise fashion. The first step is to solve for the solution of each elemental time slice. Then, the elemental solutions are integrated for the complete result. This method was chosen because a simple analytical solution is obtainable for the time slices, as follows.

For any particular value of *s*, the above function is nonzero for only an instant when the independent variable *t* is equal to *s*. The contribution from that instant u_S may be treated as a boundary value problem in which the initial value of u_S is given. Since the source term is zero thereafter, we may neglect the source term in the diffusion equation, giving

$$\left(\nabla^2 u_s\right)\alpha^2 - \gamma^2 u_s = \frac{\partial}{\partial t} u_s \quad , \tag{2.17}$$

which has a solution of the form

$$u_s = \int_{-\infty}^{\infty} (Y\ T)\, d\, k \quad , \tag{2.18}$$

where the separable component solutions are of the form

$$Y = B\ e^{i\, y\, k} \quad , \tag{2.19}$$

$$T = \begin{cases} 0 & (t-s<0) \\ e^{-(t-s)w^2} & (t-s \geq 0) \end{cases} \quad . \tag{2.20}$$

Substituting from Eqs. (2.19) and (2.20) into (2.18), and then into (2.17), the following relationship is found for the variables *k* and *w*.

$$w^2 = \alpha^2 k^2 + \gamma^2 \quad . \tag{2.21}$$

The boundary condition is that, at the instant when $t-s=0_+$, the value of u_s is simply equal to the source function at t=s. Recognizing that Eq. (2.8) is a Fourier integral, the coefficient *B* may be expressed as the inverse Fourier transform of the source function

$$B = \frac{1}{2\pi}\left(\int_{-\infty}^{\infty} e^{-\left[\frac{cs+y}{a}\right]^2 - c\beta s - iky} \, dy \right) \quad . \tag{2.22}$$

The solution is

$$B = \frac{1}{2}\frac{a\, e^{-\frac{1}{4}a^2k^2 + c(ik-\beta)s}}{\sqrt{\pi}} \quad . \tag{2.23}$$

Substituting into Eq. (2.19) and then (2.18) and solving, the result is

$$u_s = \frac{a}{\sqrt{4\alpha^2(-s+t)+a^2}} e^{-\gamma^2(-s+t) - \frac{(cs+y)^2}{4\alpha^2(-s+t)+a^2} - c\beta s} \quad . \tag{2.24}$$

The total solution for energy density is found from integrating over all time slices up to the time *t*,

$$u = \int_0^t u_s \, d s \quad . \tag{2.25}$$

Of particular interest is the energy flux towards the water/sediment interface, at y=0, which is given by Eq. (2.1). Furthermore, if the interface is modeled as an energy sink, we may construct an antisymmetric source in the upper half-space, which has the effect of doubling the energy flux. Thus, substituting from Eq. (2.25) into (2.1) and multiplying by 2, an expression for the energy flux as a function of time is obtained,

$$E(t) = 2\left(\int_0^t \left[-\alpha^2 \frac{\partial}{\partial y} u_s \right] d s \right) \text{ at } y=0 \quad . \tag{2.26}$$

Substituting from Eq. (2.24) for u_s, the final solution is given by the integral

$$E(t) = 4\left(\int_0^t \frac{a c \alpha^2 s \, e^{-\gamma^2[-s+t] - \frac{c^2 s^2}{4\alpha^2[-s+t]+a^2} - c\beta s}}{\left[4\alpha^2\{-s+t\}+a^2\right]^{\frac{3}{2}}} d s \right) . \tag{2.27}$$

This integral does not have a simple analytical solution, and therefore it was computed numerically. The integrand is monotonic and simple to integrate accurately.

If we make the assumption that the diffusion constant is small such that $4\alpha^2(-s+t)+a^2$ may be approximated by a^2, then a simpler approximate solution is possible. Let E_a denote the approximate solution

$$E_a(t) = 4\left(\int_0^t \frac{c \alpha^2 s \, e^{-\gamma^2[-s+t] - \frac{c^2 s^2}{a^2} - c\beta s}}{a^2} d s \right) , \tag{2.28}$$

which can be solved in terms of error functions.

The total energy input per unit area is given by

$$I = \int_0^{\infty} \left(\int_{-\infty}^{\infty} \left(\int_{-\infty}^{\infty} F \, dt \right) dy \right) d s = \frac{a \sqrt{\pi}}{\beta c} \quad . \qquad (2.29)$$

The integration with respect to y should strictly be between -∞ and zero. For simplicity, the limits were extended to + and - ∞, so that an error function may be avoided. The result is an overestimation of the input energy by a fraction of approximately $a\beta$. Assuming that the pulse width a is small compared to the decay constant $1/\beta$, the error will be small. Substituting into Eq. (2.15), the scattered power/unit solid angle/unit area/unit energy input is given by

$$S_e(t) = \frac{E(t)}{I} \phi(\theta_i) \left[\sin[\theta_i] \frac{2 \sin[\theta_o]}{2\pi} \right] \quad . \qquad (2.30)$$

2.3 INPUT PARAMETERS

The diffusion coefficient is the central parameter in this model although it does not directly determine the scattering strength. In Eq. (2.15) it is seen that in the limit that the diffusion coefficient α^2 tends to infinity, the scattering strength saturates at an asymptotic value, whereby all the incident energy is scattered back into the water. For gases, the value of α^2 is given by

$$\alpha^2 = dc/3 \quad , \qquad (2.31)$$

where d is the mean free path, and c the average speed of particles. If we assume that diffuse sound energy is transmitted from a sediment grain to its neighbors in a similar manner, then the mean free path d should be equal to the mean grain diameter, and c to the speed of sound. Biot's theory shows that there can be more than one sound speed in a porous sediment. For simplicity, let us make the assumption that speed of energy transport can be approximated

by a single value, and that this value is approximately equal to the fast wave speed, which in sand is typically in the region of 1700 m/s.

The loss parameter γ^2 represents the rate at which the diffuse acoustic energy is converted into other forms of energy. This rate may have some relationship to the rate at which energy is attenuated from the coherent acoustic wave. Therefore, it is more insightful to define γ^2 in terms of a ratio R_γ such that

$$R_\gamma = \gamma^2 / (c\,\beta_n) \quad , \tag{2.32}$$

where c is the speed in meters per second, and β_n is the intensity attenuation coefficient, in Nepers per meter, of a coherent plane wave traveling through the sediment; 4.343 β_n is equal to the plane wave attenuation in decibels per meter. The value of R_γ must be greater than or equal to zero. At zero, energy is losslessly diffused; at infinity, all diffuse energy is completely absorbed by the medium.

The attenuation β of the source function is simply the decay rate of the plane wave intensity in the vertical direction. At normal incidence it is equal to β_n, the attenuation coefficient of the plane wave intensity in Nepers per meter. At other angles, it is equal to β_n divided by the sine of the transmission angle, measured relative to the horizontal.

The transmission coefficient for sandy sediments is obtained from Biot's theory. It will not be derived here because it has been adequately covered in readily available references.[8]

This page intentionally left blank.

3. COMPARISON WITH EXPERIMENTAL DATA

A comparison of the model predicted backscattering strength will be made with Lambert's rule, and then with backscattering strengths measured by Nolle et al. Finally, the temporal nature of the modeled backscatter will be compared with new experimental data at normal incidence.

3.1 COMPARISON WITH EXPERIMENTAL DATA FROM NOLLE et al.

The experiments of Nolle et al. were done with well-graded sand samples and narrowband signals. Therefore they are directly comparable with the theoretical results for discrete frequencies and grain sizes. The attenuation and transmission coefficients, β_n and $\phi(\theta_i)$, of the coherent plane wave entering the sediment were computed using the procedure described by Chotiros[9] and the values in Table 3.1. The parameter values used to compute the diffusion constant α^2 are shown in Table 3.2. Little is known about the absorption ratio R_γ. The diffusion model does not have any means for estimating it from measurable physical properties, aside from bounding its value between zero and infinity. By adjusting the value of R_γ, the model, as expressed in Eq. (2.15), could be adjusted to fit the backscattering strength measurements. The model and experimental results at 500 kHz on sand samples of four different grain sizes are shown in Fig. 3.1. For wavelength-to-grain size ratios less than 10, the model reaches saturation, and consistently underestimated the measured backscattering strength. This does not necessarily mean that the model is invalid; it is likely that a stronger scattering mechanism has taken over. Geometric scattering by grain facets, particularly those at the water/sediment interface, is the most likely culprit. A similar set of results for a frequency of 1 MHz are shown in Fig. 3.2.

From these results, an empirical relationship between the dimensionless absorption ratio R_γ and the wavelength-to-grain size ratio was obtained, as shown in Fig. 3.3; in computing wavelength, the fast wave speed (1700 m/s) was assumed. Both the 500 kHz and 1 MHz data appear to fall on one continuous curve. The value of R_γ is close to zero for wavelength-to-grain size

Table 3.1
Water and water-saturated sand poroelastic parameters.

Parameter	Value	Units
Solid phase parameters		
Density	2650	kg/m^3
Bulk modulus	7.00E+09	Pa
Fluid phase parameters		
Density	1000	kg/m^3
Bulk modulus	2.25E+09	Pa
Viscosity	1.00E-03	kg/m-s
Frame parameters		
Porosity	0.36	-
Shear modulus	2.61E+07	Pa
Shear log decrement	0.15	-
Bulk modulus	5.30E+09	Pa
Bulk log decrement	0.15	-

Table 3.2
Diffusion parameters.

Parameter	Symbol	Value	Units
Transport speed	*c*	1700	m/s
Grain size: sample 1	*d*	0.000115	m
Grain size: sample 2	*d*	0.000164	m
Grain size: sample 3	*d*	0.00038	m
Grain size: sample 4	*d*	0.00065	m

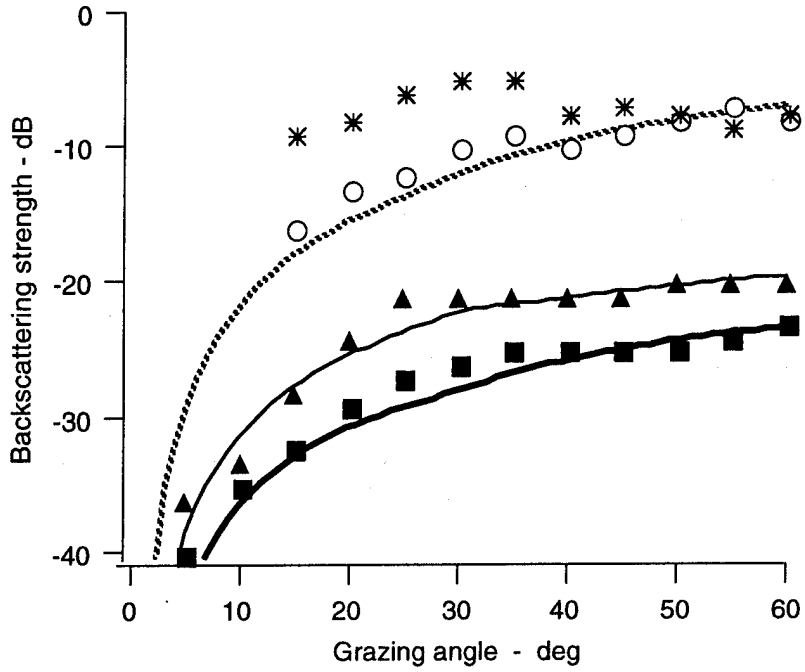

Experiment	Theory	Wavelength / Grain size	R_γ
✳	⋯⋯	5	0.0
○	⋯⋯	9	0.0
▲	——	21	2.0
■	——	30	4.0

Figure 3.1
Fitting of model backscattering strength curves to experimental data (Nolle et al.) at 500 kHz by adjusting $R\gamma$.

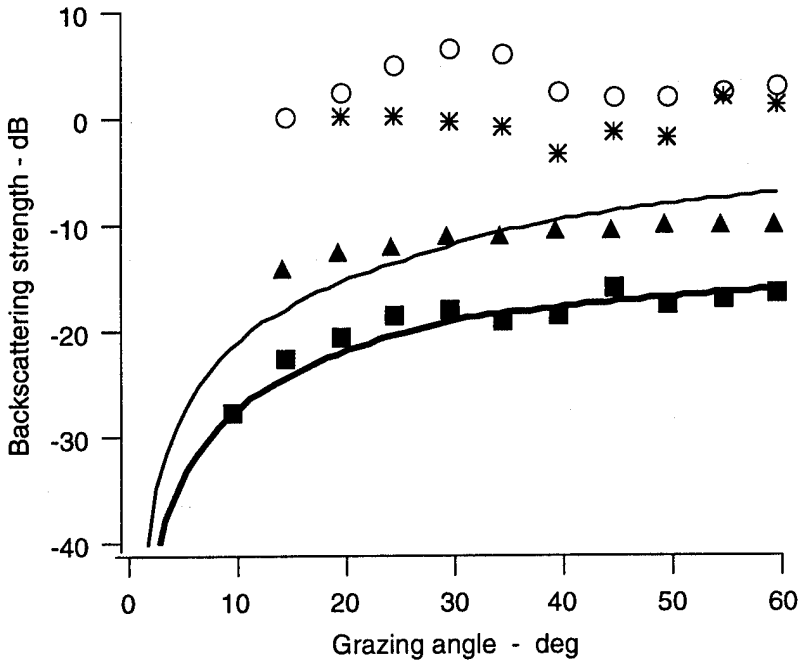

Experiment	Theory	Wavelength / Grain size	R_γ
✳	———	2.6	0.0
○	———	4.5	0.0
▲	———	10.4	0.0
■	———	14.8	0.5

Figure 3.2
Fitting of model backscattering strength curves to experimental data (Nolle et al.) at 1 MHz by adjusting $R\gamma$.

ratios less than 10; at higher values of wavelength-to-grain size ratio, R_γ appears to increase linearly.

3.2 COMPARISON WITH LAMBERT'S RULE

Using Eq. (2.15), the parameter values in Tables 3.1 and 3.2, and the relationship found between R_γ and wavelength-to-grain size ratio shown in Fig. 3.3, backscattering strength versus grazing angle curves were computed for a wide range of typical cases. For example, the scattering strength curves at 1, 10, 100, and 1000 kHz were computed for a sandy sediment with a grain size of 0.1 mm. In each case, a Lambert's rule curve was compared to the diffusion model. The results are shown in Fig. 3.4. In all cases, it is apparent that Lambert's rule is a good fit at grazing angles less than about 30°. It is also clear that at 10 kHz, which corresponds to a wavelength-to-grain size ratio of 14782, the backscattering strength is very small. Therefore, it may be concluded that the diffusion model is likely to be significant for wavelength-to-grain size ratios between 10 and 10,000. Above and below these limits, it is expected to be overshadowed by other scattering mechanisms.

3.3 COMPARISON OF DECAY TIME WITH NEW EXPERIMENTAL MEASUREMENTS

A unique feature of the diffusion model is that it predicts a certain lag between the reflected and scattered signals, which is a function of the propagation speed and mean-free-path. While many models can be fitted to the backscattering strength versus grazing angle curves, few are able to give any insight into the time dependence of the scattered signal. The time dependence is most clearly seen in the scattering of a short plane wave pulse at normal incidence. An experiment was performed with a wideband transducer. A narrowbeam signal was used to approximate a bounded plane wave. Pulse compression filtering was applied to the received signal to achieve an approximately Gaussian pulse, with a time constant of 3.3 ms, at a center frequency of approximately 150 kHz. Ten pings were collected from different parts of a smoothed sand surface. The sand had been degassed and compacted by vibration. The coherent part of the echo is the average of the ten pings. The

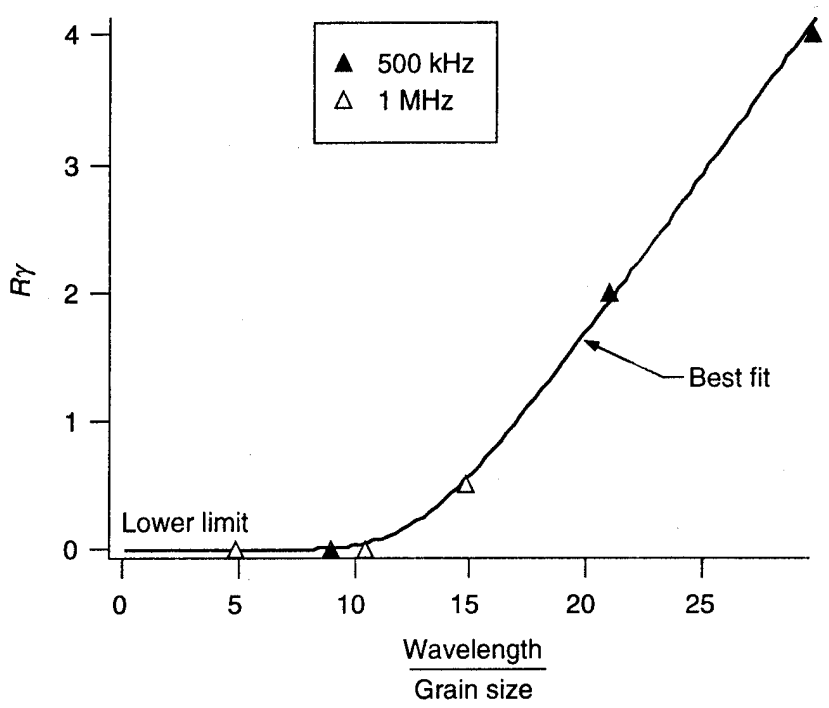

Figure 3.3
Relationship between wavelength-to-grain size ratio and the absorption ratio $R\gamma$ deduced from matching diffusion model of backscattering to the experimental data of Nolle et al.

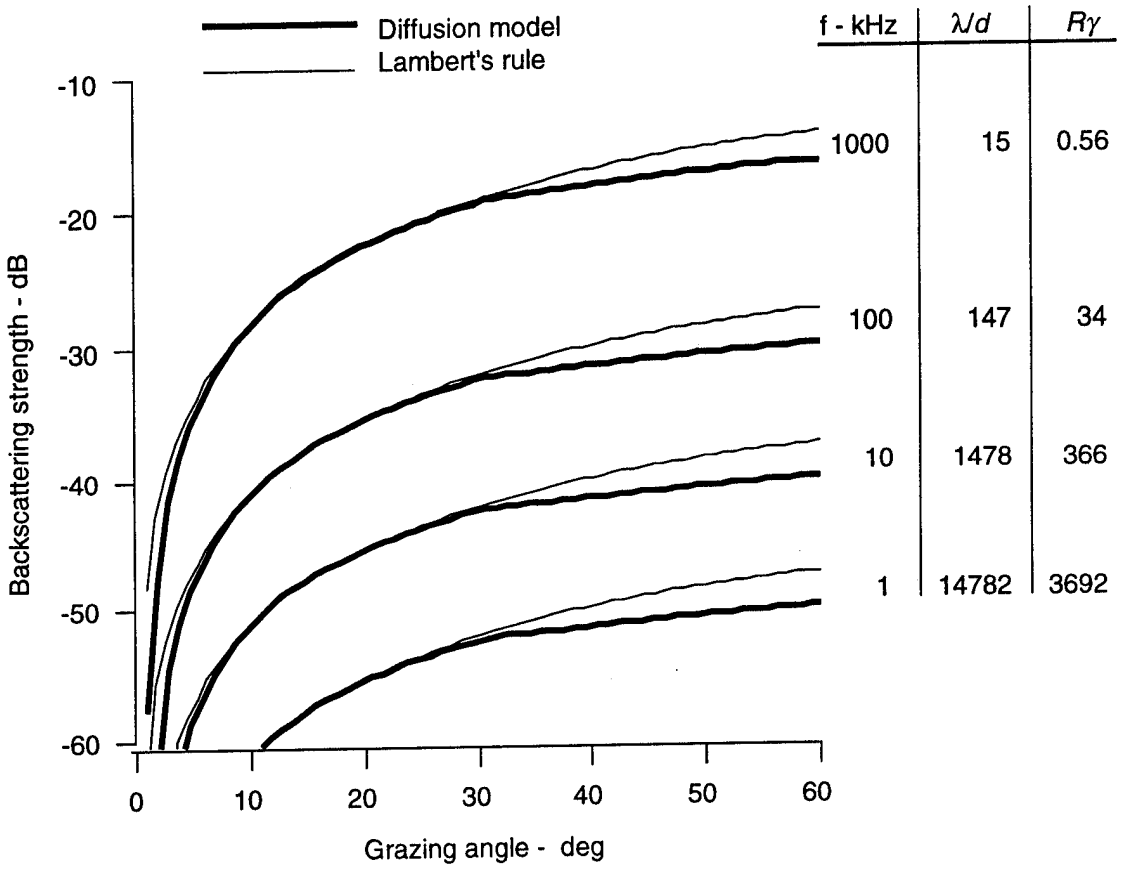

Figure 3.4
Example of comparison between Lambert's rule and diffusion theory.

scattered component is computed from the rms difference between the individual pings and the average.

This experiment is different from that of Nolle et al. in two ways: (1) a broadband signal was used in order to achieve a short signal pulse, and (2) the sand was not graded and contained grains of various sizes. Assuming that the grain and wavelength effects add in a mean-square sense, the response of the sand to a broadband signal may be estimated by convolving $E(t)$ with the density functions of the grain size $p_q(q)$ and signal spectrum $p_f(f)$, where q is grain size in ϕ, and f is frequency in Hertz. The final result $E_c(t)$ is then given by the following convolution integral.

$$E_c(t) = \int_0^{\infty} \left(\int_{-\infty}^{\infty} p_q[q] E[t] \, dq \right) p_f(f) \, df \quad . \qquad (3.1)$$

The cumulative distribution function of the grain size was measured at intervals of 1ϕ and a normal distribution function was fitted to it, as shown in Fig. 3.5, from which $p_q(q)$ was calculated. The acoustic signal was digitally filtered and the resulting spectral density function of signal spectrum $p_f(f)$ as shown in Fig. 3.6. These functions were used to numerically compute Eq. (3.1), in conjunction with the parameter values in Tables 3.1 and 3.2, and values of R_y as a function of wavelengths-to-grain size ratio as shown in Fig. 3.4.

The theoretical and experimental results are shown in Fig. 3.7. The signal envelopes are plotted on a decibel scale. The theoretical and experimental results appear to be consistent for the most part. The disagreement is mostly in the vicinity of t=0, and this is likely caused by an edge effect that has been ignored in the theoretical model; the model assumes that the pulse is a fully formed Gaussian shaded function, as stated in Eq. (2.16). In reality, at t=0 only half the pulse has entered the sediment, and there are likely to be further complications due to surface effects. The model appears to overestimate the scattered signal in the vicinity of t=0. The apparent peak in the experimental measurements of the random component of backscatter about t=0 should be ignored because it is most likely caused by surface scattering, due to

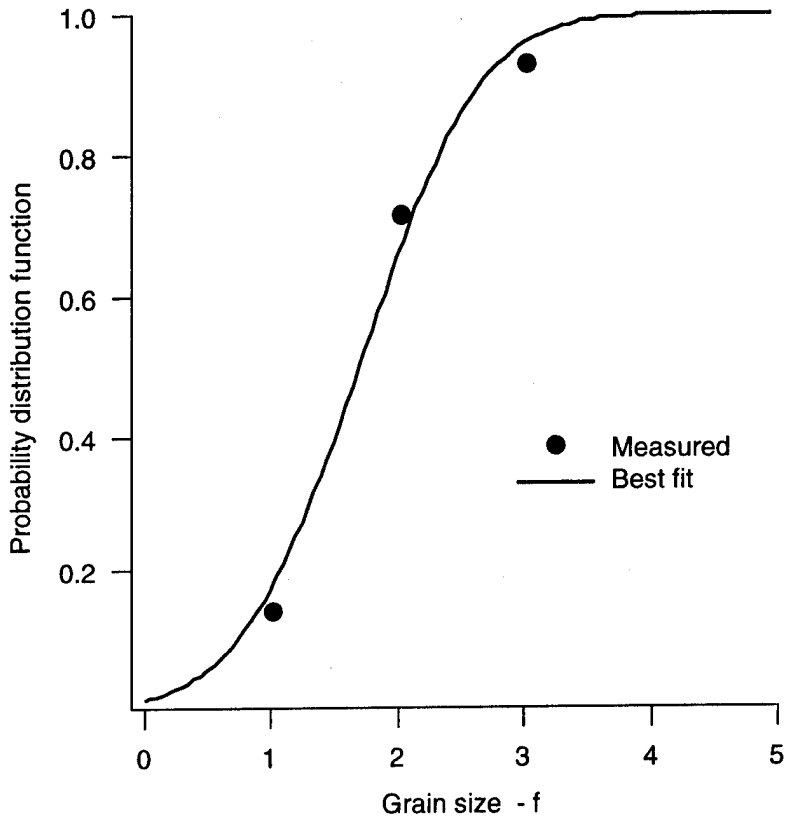

Figure 3.5
Measured cumulative distribution of grain sizes and best fit normal probability distribution (mean = 1.7ϕ, standard deviation = 0.75ϕ).

ARL - UT
AS-95-1226
NPC/RFO
12-95/svr

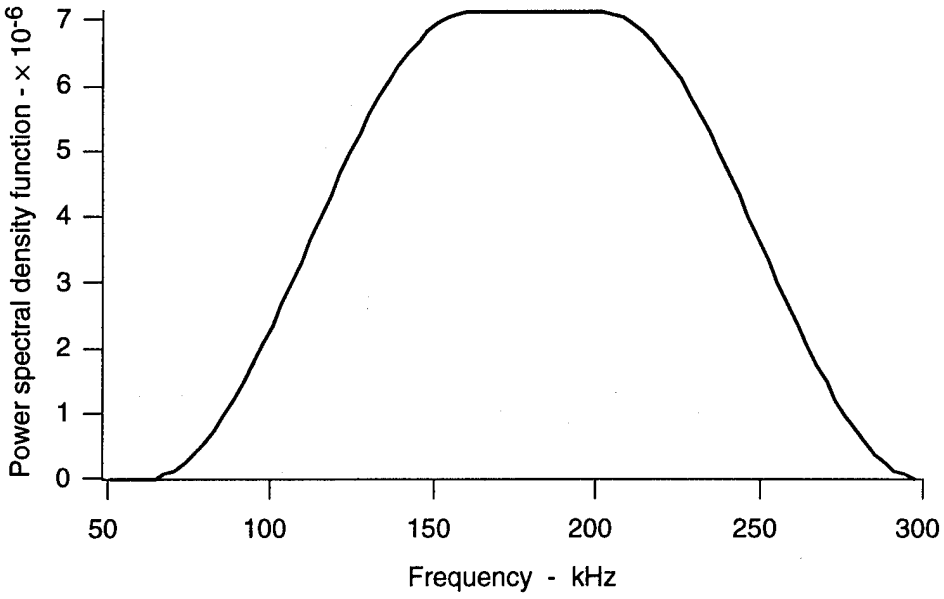

Figure 3.6
Power spectral density function of acoustic signal.

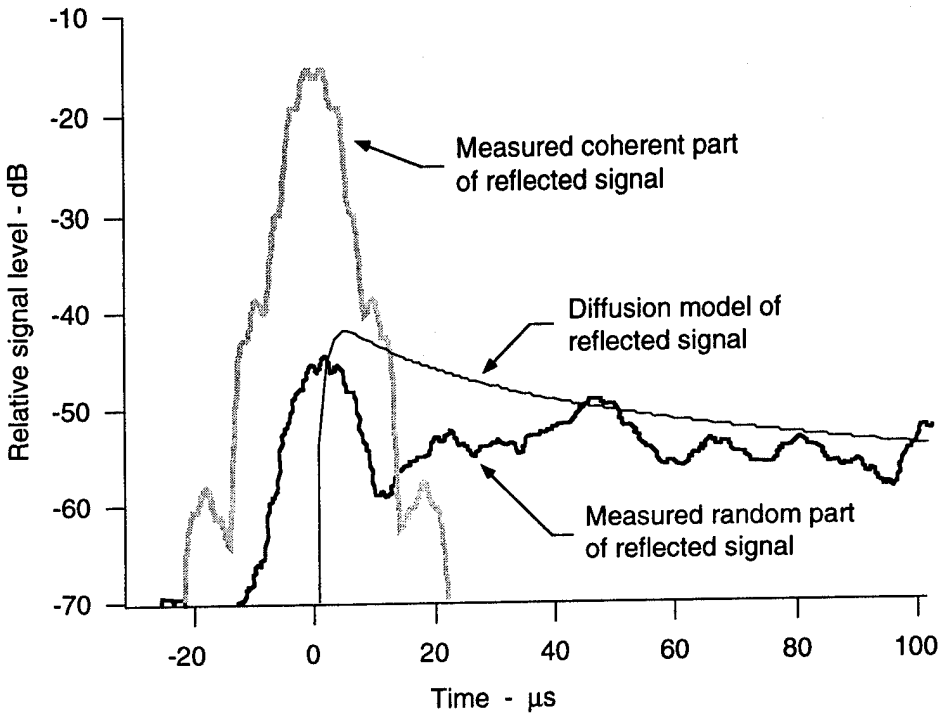

Figure 3.7
Comparison of diffusion model with random part of measured reflected signal at normal incidence from a smooth sand surface.

residual surface roughness. The experimental data are only valid up to $t = 100$ μs, because multipaths within the water column begin to appear at this point. Generally, the model and experimental data are in agreement.

This page intentionally left blank.

4. CONCLUSIONS

A scattering model from water-saturated sand with a smooth surface, based on the diffusion theory, was developed. It is applicable to acoustic scattering from sandy ocean sediments. It has the following features.

(1) Scattering strength versus grazing angle curve closely resembles Lambert's rule.

(2) Its predictions can be closely matched to laboratory measurements by Nolle et al.

(3) The comparison with experimental data yielded a tentative relationship between the absorption and the wavelength-to-grain size ratios, which indicated that scattering by diffusion is expected to be significant for wavelength-to-grain size ratios between 10 and 10,000.

(4) The temporal characteristics of the scattered signal are consistent with new experimental data, in which the random part of the signal was detected and found to be consistent with the model prediction in both amplitude and decay constant.

(5) Since a large proportion of shallow water regions of the globe are sandy, this model is expected to be a significant component in a comprehensive bottom scattering model for modeling high frequency sonar systems.

This research project is closely related to another basic research project sponsored by ONR Code 321OA, to extend Biot's theory for the purpose of modeling scattering by sediment grains. It is expected that when the ONR sponsored project is completed, it will supply a sound basis for computation of the input parameters for the diffusion model.

The model for multiple scattering by sediment grains developed in this report will be transitioned into the larger bottom scattering model currently being assembled, under the MTEDS project. The total model contains components developed in past basic research projects sponsored by the NRL High Frequency

Acoustics Program over the past five years, including the model for scattering by sediment gas bubbles. The final objective is to obtain OAML certification.

ACKNOWLEDGMENTS

The experiments were conducted with the able assistance of Joe Molis, ARL:UT.

The work was funded by the High Frequency Acoustics Program of the Naval Research Laboratory, Stennis Space Center (NRL/SSC). Thanks are due to Steve Stanic and Dan Ramsdale for their encouragement and support.

This page intentionally left blank.

REFERENCES

1. A. W. Nolle, W. A. Hoyer, J. F. Mifsud, W. R. Runyan, and M. B. Ward, "Acoustical Properties of Water-filled Sands," J. Acoust. Soc. Am. 35(9), 1394-1408 (1963).

2. P. Mourad and D. R. Jackson, "High Frequency Sonar Equation Models for Bottom Backscatter and Forward Loss," Proc. OCEANS89, IEEE Publication No. 89CH2780-5, 1168-1175, 1989.

3. D. R. Jackson, S. P. Winebrenner, and A. Ishimaru, "Application of Composite Roughness Model to High-frequency Bottom Backscattering," J. Acoust. Soc. Am. 79(5), 1410-1422 (1986).

4. P. C. Hines, "Theoretical Model of Acoustic Backscatter from a Smooth Seabed," J. Acoust. Soc. Am. 88(1), 324-344 (1990).

5. L. Schwarz and T. J. Plona, "Ultrasonic Propagation in Close Packed Disordered Suspension," J. App. Phys. 55, 3971-3977 (1984).

6. Richard L. Weaver, Wolfgang Sachse, K. Green, and Y. Zhang, "Diffuse Ultrasound in Polycrystalline Solids," in Proc. Ultrasonic International 91 (Butterworth-Heinemann, Oxford, UK, 1991).

7. Richard L. Weaver, "Laboratory Studies of Diffuse Waves in Plates," J. Acoust. Soc. Am. 79, 919-923 (1986).

8. N. P. Chotiros, "Biot Model of Sound Propagation in Water-saturated Sand," J. Acoust. Soc. Am. 97(1), 199-214 (1995).

This page intentionally left blank.

26 October 1995

DISTRIBUTION LIST FOR
ARL-TR-95-30
Final Report under Contract N00039-91-C-0082, TD No. 01A2082
Volume Backscatter from Sand Grains

Copy No.	
	Commanding Officer Naval Research Laboratory Stennis Space Center, MS 39529-5004
1 - 3	Attn: D. Ramsdale (Code 7170)
4	S. Stanic (Code 7174)
5	D. Lott (Code 7431)
6	E. Franchi (Code 7100)
7	S. Tooma (Code 7430)
8	M. Richardson (Code 7431)
9	R. Meredith (Code 7174
10	Library (Code 7032.2)
	The Office of Naval Research San Diego Regional Office 4520 Executive Drive, Suite 300 San Diego, CA 92121-3019
11	Attn: J. Starcher (ACO)
	Director Naval Research Laboratory Washington, DC 20375
12	Attn: Code 2627
13	B. Houston (Code 5136)
	DTIC-OCC Defense Technical Information Center 8725 John J. Kingman Road, Suite 0944 Fort Belvoir, VA 22060-6218
14 - 25	Attn: Library
	Director Research Program Department Office of Naval Research Ballston Tower One 800 North Quincy Street Arlington, VA 22217-5000
26	Attn: J. Simmen (Code 321)
27	E. Chaika (Code 322)
28	W. Ching (Code 321)
29	T. Goldsberry (Code 322)
30	D. Houser (Code 333)

Distribution List for ARLTR-95-30 under Contract N00039-91-C-0082, TD No. 01A2082 (cont'd)

Copy No.	
	Commander Naval Meteorology and Oceanography Command Stennis Space Center, MS 39522-5000
31	Attn: D. Durham (N5A)
32	R. Martin (N5C)
	Commander Program Executive Office - Mine Warfare Crystal Plaza Bldg. 6 2531 Jefferson Davis Highway Arlington, VA 22242-5167
33	Attn: J. Grembi (PEOMIW)
34	D. Gaarde (PMO407B)
	G & C Systems Manager MK48/ADCAP Program Office National Center 2 2521 Jefferson Davis Hwy., 12W32 Arlington, VA 22202
35	Attn: H. Grunin (PMO402E1)
	Program Manager MK50 Torpedo Program Office Crystal Park 1 2011 Crystal Drive, Suite 1102 Arlington, VA 22202
36	Attn: A. Knobler (PMO406B)
	Commander Dahlgren Division Naval Surface Warfare Center Dahlgren, VA 22448-5000
37	Attn: Library
	Commander Dahlgren Division Naval Surface Warfare Center Silver Spring, MD 20903-5000
38	Attn: S. Martin (G94)
39	J. Sherman (N50)
40	M. Stripling (N04W)

Distribution List for ARLTR-95-30 under Contract N00039-91-C-0082, TD No. 01A2082 (cont'd)

Copy No.	
	Director Applied Physics Laboratory The University of Washington 1013 NE 40th Street Seattle, WA 98105
41	Attn: R. Spindel
42	D. Jackson
43	K. Williams
44	S. Kargl
	Director Life Sciences Directorate Office of Naval Research Arlington, VA 22217-5000
45	Attn: S. Zornetzer (Code 114)
	Director Marine Physical Laboratory The University of California, San Diego San Diego, CA 92152
46	Attn: K. Watson
47	C. de Moustier
	Commander Mine Warfare Command 325 Fifth St. SE Corpus Christi, TX 78419-5032
48	Attn: G. Pollitt (N02R)
	Applied Research Laboratory The Pennsylvania State University P.O. Box 30 State College, PA 16804-0030
49	Attn: L. Hettche
50	R. Goodman
51	E. Liszka
52	Library
53	D. McCammon
54	F. Symons

Distribution List for ARLTR-95-30 under Contract N00039-91-C-0082, TD No. 01A2082 (cont'd)

Copy No.	
	National Center for Physical Acoustics University of Mississippi Coliseum Drive University, MS 38677
55	Attn: J. Sabatier
	Commanding Officer Coastal Systems Station, Dahlgren Division Naval Surface Warfare Center Panama City, FL 32407-5000
56	Attn: M. Hauser (Code 10CD)
57	R. Lim (Code 130B)
58	E. Linsenmeyer (Code 10P)
59	D. Todoroff (Code 130)
	Commander Naval Undersea Warfare Center Division New London, CT 06320-5594
60	Attn: J. Chester (Code 3112)
61	P. Koenig (Code 33A)
	Advanced Research Projects Agency 3701 North Fairfax Drive Arlington, VA 22203-1714
62	Attn: W. Carey
	Commander Naval Undersea Warfare Center Division Newport, RI 02841-5047
63	Attn: J. Kelly (Code 821)
64	F. Aidala (Code 842)
65	W. Gozdz (Code 843)
	Physics Department The University of Texas at Austin Austin, TX 78712
66	Attn: T. Griffy
	Aerospace Engineering Department The University of Texas at Austin Austin, TX 78712
67	Attn: M. Bedford
68	M. Stern

Distribution List for ARLTR-95-30 under Contract N00039-91-C-0082, TD No. 01A2082 (cont'd)

Copy No.	
69	Robert A. Altenburg, ARL:UT
70	Hollis Boehme, ARL:UT
71	Frank A. Boyle, ARL:UT
72	Nicholas P. Chotiros, ARL:UT
73	John M. Huckabay, ARL:UT
74	Thomas G. Muir, ARL:UT
75	Library, ARL:UT
76 - 81	Reserve, ARL:UT